Closed Timelike Curves Induced by a Buchdahl-Inspired Vacuum Spacetime in $\mathcal{R}^2$ Gravity

Hoang Ky Nguyen [1,*] and Francisco S. N. Lobo [2,3]

[1] Department of Physics, Babeş–Bolyai University, 400084 Cluj-Napoca, Romania
[2] Instituto de Astrofísica e Ciências do Espaço, Faculdade de Ciências da Universidade de Lisboa, Campo Grande, Edifício C8, 1749-016 Lisbon, Portugal; fslobo@fc.ul.pt
[3] Departamento de Física, Faculdade de Ciências da Universidade de Lisboa, Campo Grande, Edifício C8, 1749-016 Lisbon, Portugal
[*] Correspondence: hoang.nguyen@ubbcluj.ro

Abstract: The recently obtained *special* Buchdahl-inspired metric Phys. Rev. D 107, 104008 (2023) describes asymptotically flat spacetimes in pure Ricci-squared gravity. The metric depends on a new (Buchdahl) parameter $\tilde{k}$ of higher-derivative characteristic, and reduces to the Schwarzschild metric, for $\tilde{k} = 0$. For the case $\tilde{k} \in (-1, 0)$, it was shown that it describes a traversable Morris–Thorne–Buchdahl (MTB) wormhole Eur. Phys. J. C 83, 626 (2023), where the weak energy condition is formally violated. In this paper, we briefly review the *special* Buchdahl-inspired metric, with focuses on the construction of the Kruskal–Szekeres (KS) diagram and the situation for a wormhole to emerge. Interestingly, the MTB wormhole structure appears to permit the formation of closed timelike curves (CTCs). More specifically, a CTC straddles the throat, comprising of two segments positioned in opposite quadrants of the KS diagram. The closed timelike loop thus passes through the wormhole throat twice, causing *two* reversals in the time direction experienced by the (timelike) traveller on the CTC. The key to constructing a CTC lies in identifying any given pair of antipodal points (T, X) and $(-T, -X)$ *on the wormhole throat* in the KS diagram as corresponding to the same spacetime event. It is interesting to note that the Campanelli–Lousto metric in Brans–Dicke gravity is known to support two-way traversable wormholes, and the formation of the CTCs presented herein is equally applicable to the Campanelli–Lousto solution.

Keywords: closed timelike curves; Ricci-squared gravity; traversable wormholes

1. Introduction

Wormholes are hypothetical shortcuts in spacetime, and are solutions for the gravitational field equations, where the fundamental ingredient is the flaring-out condition [1]. In classical General Relativity, the latter condition entails the violation of the null energy condition, and consequently all of the energy conditions [2,3]. However, it has been shown that in modified theories of gravity, the matter threading the wormhole throat may satisfy the energy conditions, and it is the higher order curvature terms, interpreted as a gravitational fluid, that support these nonstandard wormhole geometries [4,5]. Another extremely interesting feature of traversable wormholes is that they may be hypothetically manipulated to induce closed timelike curves (CTCs) [6–9]. In fact, General Relativity is contaminated with non-trivial geometries, which generate CTCs [10–18], which allow time travel, in the sense that an observer that travels on a trajectory in spacetime along this curve and may return to an event before his departure [19].

Due to the interesting physics involved in these exotic spacetimes, much attention has been given to these geometries in the literature, and we refer the reader to [3], and the references therein, for a recent review. As wormhole physics has been explored extensively in modified theories of gravity, where the higher-order curvature terms support these

wormhole geometries [5], in this work, we shall be interested in the recent *special* Buchdahl-inspired metric, obtained by one of the present authors [20], that describes asymptotically flat spacetimes in pure $\mathcal{R}^2$ gravity [21]. The metric is dependent on a new (Buchdahl) parameter $\tilde{k}$ of higher-derivative characteristic, and recovers the Schwarzschild metric when $\tilde{k} = 0$. In a recent work [22], it was demonstrated that the *special* Buchdahl-inspired metric supports a two-way traversable Morris–Thorne–Buchdahl (MTB) wormhole for $\tilde{k} \in (-1, 0)$, in which case the weak energy condition is formally violated.

In this paper, we shall review the *special* Buchdahl-inspired metric, with focuses on the construction of the ζ–Kruskal–Szekeres (KS) diagram and the conditions to generate a wormhole. Curiously, the MTB wormhole structure appears to permit the formation of CTCs. A CTC straddles the throat, comprising of two segments positioned in the opposite Quadrant I and Quadrant III of the ζ–KS diagram. The closed timelike loop thus passes through the wormhole throat twice, causing *two* reversals in the time direction experienced by the (timelike) traveller on the CTC. The key to constructing a CTC lies in identifying any given pair of antipodal points (T, X) and $(-T, -X)$ *on the wormhole throat* in the ζ–KS diagram as corresponding to the same spacetime event.

In a previous work [23], Popławski put forth this procedure for the Einstein–Rosen bridge in which he identified antipodal points *on the horizon* as corresponding to the same spacetime event. Although his maneuver may prove untenable for "Schwarzschild wormholes" (and he did not report a CTC), we adapt his construction to the MTB wormhole, with a minor but crucial *modification*: instead of the horizon, the identification of antipodal points takes place on the wormhole throat which permits a two-way traversal. In certain situations, the Campanelli–Lousto solution in Brans–Dicke gravity is known to support two-way traversable wormholes [24]. When this occurs, the formation of CTCs presented herein is equally applicable to the Campanelli–Lousto solution. Generally speaking, our CTC should be a generic aspect of the family of scalar–tensor theories.

This paper is organized in the following manner: In Section 2, we present the vacuum *special* Buchdahl-inspired metric, and in Sections 3 and 4, we review the causal structure of the solution, using the Kruskal–Szekeres diagram, which is a maximal analytic extension of the *special* Buchdahl-inspired metric. For completeness, Section 5 provides a brief detour for the case of naked singularities. Section 6, the most essential one, describes our construction of the CTCs for the MTB wormholes. Finally, in Section 7, we discuss our results and conclude.

2. The *Special* Buchdahl-Inspired Metric: Brief Review

The pure $\mathcal{R}^2$ action, $\int d^4x \sqrt{-g}\, \mathcal{R}^2$, yields the field equation in vacuo [21]

$$\mathcal{R}\left(\mathcal{R}_{\mu\nu} - \frac{1}{4}g_{\mu\nu}\mathcal{R}\right) + g_{\mu\nu}\Box\mathcal{R} - \nabla_\mu\nabla_\nu\mathcal{R} = 0. \tag{1}$$

Despite the fourth-order nature of this equation, in [20], one of the present authors obtained an exact closed analytical solution, named the *special* Buchdahl-inspired metric. It describes a static and spherically symmetric vacuum configuration

$$ds^2 = \left|1 - \frac{r_{\rm s}}{r}\right|^{\tilde{k}}\left\{-\left(1 - \frac{r_{\rm s}}{r}\right)dt^2 + \left(\frac{\rho(r)}{r}\right)^4 \frac{dr^2}{1 - \frac{r_{\rm s}}{r}} + \left(\frac{\rho(r)}{r}\right)^2 r^2 d\Omega^2\right\}, \tag{2}$$

where the function $\rho(r)$ is given by virtue of

$$\left(\frac{\rho(r)}{r}\right)^2 := \frac{\zeta^2\left|1 - \frac{r_{\rm s}}{r}\right|^{\zeta-1}}{\left(1 - {\rm s}\left|1 - \frac{r_{\rm s}}{r}\right|^{\zeta}\right)^2}\left(\frac{r_{\rm s}}{r}\right)^2. \tag{3}$$

The dimensionless parameters $\tilde{k}$ and ζ are defined as $\tilde{k} := k/r_{\rm s}$, $\zeta := \sqrt{1 + 3\tilde{k}^2}$, and ${\rm s} := \pm 1$ denotes the *signum* of $1 - \frac{r_{\rm s}}{r}$. Here, $\tilde{k}$ is a new (Buchdahl) parameter of higher-derivative

characteristic, and $r_{\rm s}$ plays the role of a Schwarzschild radius. At $\tilde{k} = 0$, $\rho(r) \equiv r$ and Equation (2) recovers the Schwarzschild metric. At spatial infinity, metric (2) is asymptotically flat (Note: a more general solution expressed in a compact form, named the Buchdahl-inspired metric, was obtained by one of the authors in Refs. [25,26] by completing the original but unfinished work of Buchdahl [21]. This latter solution is asymptotically de Sitter, and is specified by *four* parameters, reflecting the fourth-derivative nature of a quadratic theory).

Upon another coordinate transformation [22]

$$1 - \frac{r'_{\rm s}}{r'} = {\rm s}\left|1 - \frac{r_{\rm s}}{r}\right|^{\zeta}, \tag{4}$$

in which $r'_{\rm s} := \zeta\, r_{\rm s}$ and ${\rm s} = {\rm sgn}\left(1 - \frac{r_{\rm s}}{r}\right) = {\rm sgn}\left(1 - \frac{r'_{\rm s}}{r'}\right)$, the metric given in Equations (2) and (3) can be brought into the following form

$$ds^2 = -{\rm s}\left|1 - \frac{r'_{\rm s}}{r'}\right|^{A} dt^2 + {\rm s}\left|1 - \frac{r'_{\rm s}}{r'}\right|^{B} dr'^2 + \left|1 - \frac{r'_{\rm s}}{r'}\right|^{B+1} r'^2 d\Omega^2, \tag{5}$$

where

$$A := \frac{\tilde{k} + 1}{\zeta}, \qquad B := \frac{\tilde{k} - 1}{\zeta}, \qquad \zeta := \sqrt{1 + 3\tilde{k}^2}. \tag{6}$$

The parameters satisfy the following relation:

$$A^2 + AB + B^2 = 1. \tag{7}$$

It is worth noting that the metric expressed in Equation (5) also describes the *generalized* Campanelli–Lousto (CL) solution for the Brans–Dicke action, $\int d^4x \sqrt{-g}\left[\phi\,\mathcal{R} - \frac{\omega}{\phi}\nabla^\mu \phi \nabla_\mu \phi\right]$. In the *generalized* CL metric, which was found recently in [24] by one of the present authors, A and B take on any value in $\mathbb{R}$, and are linked by

$$A^2 + AB + B^2 - 1 = -\frac{\omega}{2}(A + B)^2, \tag{8}$$

with ω being the Brans–Dicke parameter.

In the rest of this work, we shall concern ourselves with the *special* Buchdahl-inspired metric in pure $\mathcal{R}^2$ gravity. Dropping the prime in the notation of r' and $r'_{\rm s}$ in Equation (5), we shall use the explicit expression below

$$ds^2 = \left|1 - \frac{r_{\rm s}}{r}\right|^{\frac{\tilde{k}}{\zeta}}\left\{-{\rm s}\left|1 - \frac{r_{\rm s}}{r}\right|^{\frac{1}{\zeta}} dt^2 + {\rm s}\left|1 - \frac{r_{\rm s}}{r}\right|^{-\frac{1}{\zeta}} dr^2 + \left|1 - \frac{r_{\rm s}}{r}\right|^{1-\frac{1}{\zeta}} r^2 d\Omega^2\right\}, \tag{9}$$

where

$${\rm s} := {\rm sgn}\left(1 - \frac{r_{\rm s}}{r}\right), \qquad \zeta := \sqrt{1 + 3\tilde{k}^2}. \tag{10}$$

3. The ζ–Kruskal–Szekeres Coordinates

The construction of the KS diagram for the *special* Buchdahl-inspired metric has been carried out in Refs. [20,24]. However, for self-consistency and self-completeness, we summarize the key points here.

- The tortoise coordinate $r^*(r)$ for the *special* Buchdahl-inspired metric (9) is defined by virtue of

$$dr^* = \frac{{\rm s}}{\left|1 - \frac{r_{\rm s}}{r}\right|^{1/\zeta}}\, dr. \tag{11}$$

This equation is soluble, yielding the tortoise coordinate in terms of a Gaussian hypergeometric function

$$r^*(r) = \frac{r_{\rm s}}{1 - 1/\zeta}\left|1 - \frac{r_{\rm s}}{r}\right|^{1-1/\zeta} {}_2F_1\left(2, 1 - 1/\zeta; 2 - 1/\zeta; 1 - \frac{r_{\rm s}}{r}\right) - \frac{r_{\rm s}\,\pi/\zeta}{\sin(\pi/\zeta)}, \tag{12}$$

which is represented in Figure 1. The integration constant required for Equation (11) has been chosen such that $r^* = 0$ when $r = 0$.
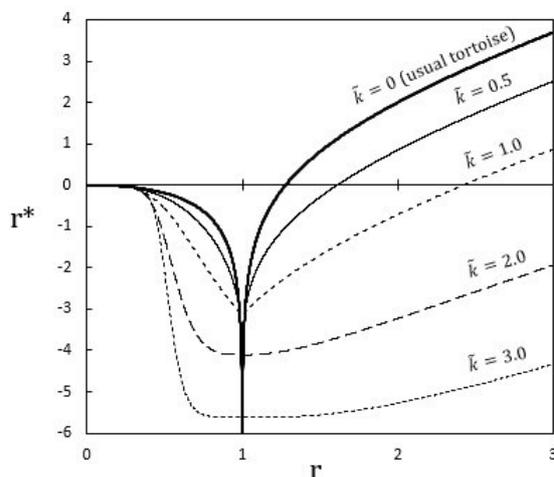

Figure 1. The ζ–tortoise coordinate given by Equation (12) for various values of $\tilde{k}$ (with $r_\mathrm{s} = 1$).

- The advanced and retarded Eddington–Finkelstein coordinates are defined as

$$v := t + r^*,\tag{13}$$

$$u := t - r^*,\tag{14}$$

respectively.

- For the Kruskal–Szekeres (KS) coordinates, it is necessary to separate the two ranges, $r > r_\mathrm{s}$ versus $r < r_\mathrm{s}$.

  – For $r > r_\mathrm{s}$, we define

$$X := \frac{1}{2}\left(e^{\frac{v}{2r_\mathrm{s}}} + e^{-\frac{u}{2r_\mathrm{s}}}\right) = e^{\frac{r^*(r)}{2r_\mathrm{s}}}\cosh\frac{t}{2r_\mathrm{s}},\tag{15}$$

$$T := \frac{1}{2}\left(e^{\frac{v}{2r_\mathrm{s}}} - e^{-\frac{u}{2r_\mathrm{s}}}\right) = e^{\frac{r^*(r)}{2r_\mathrm{s}}}\sinh\frac{t}{2r_\mathrm{s}}.\tag{16}$$

  – For $r < r_\mathrm{s}$, we define

$$X := \frac{1}{2}\left(e^{\frac{v}{2r_\mathrm{s}}} - e^{-\frac{u}{2r_\mathrm{s}}}\right) = e^{\frac{r^*(r)}{2r_\mathrm{s}}}\sinh\frac{t}{2r_\mathrm{s}},\tag{17}$$

$$T := \frac{1}{2}\left(e^{\frac{v}{2r_\mathrm{s}}} + e^{-\frac{u}{2r_\mathrm{s}}}\right) = e^{\frac{r^*(r)}{2r_\mathrm{s}}}\cosh\frac{t}{2r_\mathrm{s}}.\tag{18}$$

In combination, the *special* Buchdahl-inspired metric in the Kruskal–Szekeres (KS) coordinates is thus

$$ds^2 = \left|1 - \frac{r_\mathrm{s}}{r}\right|^{\frac{\tilde{k}}{\zeta}}\left\{-4r_\mathrm{s}^2 e^{-\frac{r^*}{r_\mathrm{s}}}\left|1 - \frac{r_\mathrm{s}}{r}\right|^{\frac{1}{\zeta}}\left(dT^2 - dX^2\right) + r^2\left|1 - \frac{r_\mathrm{s}}{r}\right|^{1-\frac{1}{\zeta}}d\Omega^2\right\},\tag{19}$$

where

$$T^2 - X^2 = -\mathrm{s}\,e^{\frac{r^*(r)}{r_\mathrm{s}}}$$

$$= -\mathrm{s}\,\exp\left[\frac{\left|1 - \frac{r_\mathrm{s}}{r}\right|^{1-1/\zeta}}{1 - 1/\zeta}\,{}_2F_1\left(2, 1 - 1/\zeta; 2 - 1/\zeta; 1 - \frac{r_\mathrm{s}}{r}\right) - \frac{\pi/\zeta}{\sin(\pi/\zeta)}\right],\tag{20}$$

$$\frac{T}{X} = \left(\tanh\frac{t}{2r_\mathrm{s}}\right)^\mathrm{s},\tag{21}$$

with s $= \pm 1$ for the ranges $r \in (r_s, \infty)$ and $r \in (-\infty, r_s)$, respectively. Note that in this final form, the coordinates T and X are *enlarged* to satisfy Equations (20) and (21). That is to say, each pair of coordinates (t, r) corresponds to *two* pairs of coordinates (T, X) and $(-T, -X)$, with X and T given by Equations (15) and (16) for the range $r \in (r_s, \infty)$ and Equations (17) and (18) for the range $r \in (-\infty, r_s)$.

It is apt and convenient to call the range $r \in (r_s, \infty)$ an "exterior" region. However, since the Kretschmann invariant in general diverges at $r = r_s$ [20], we shall avoid naming the range $r \in (0, r_s)$ an "interior" region, from here on.

4. The ζ-Kruskal–Szekeres Diagram

Restricting within the (T, X) plane, i.e., $d\theta = d\varphi = 0$, the ζ–KS diagram for metric (19) is shown in Figure 2. We refer to a number of key features, developed in Ref. [20]:
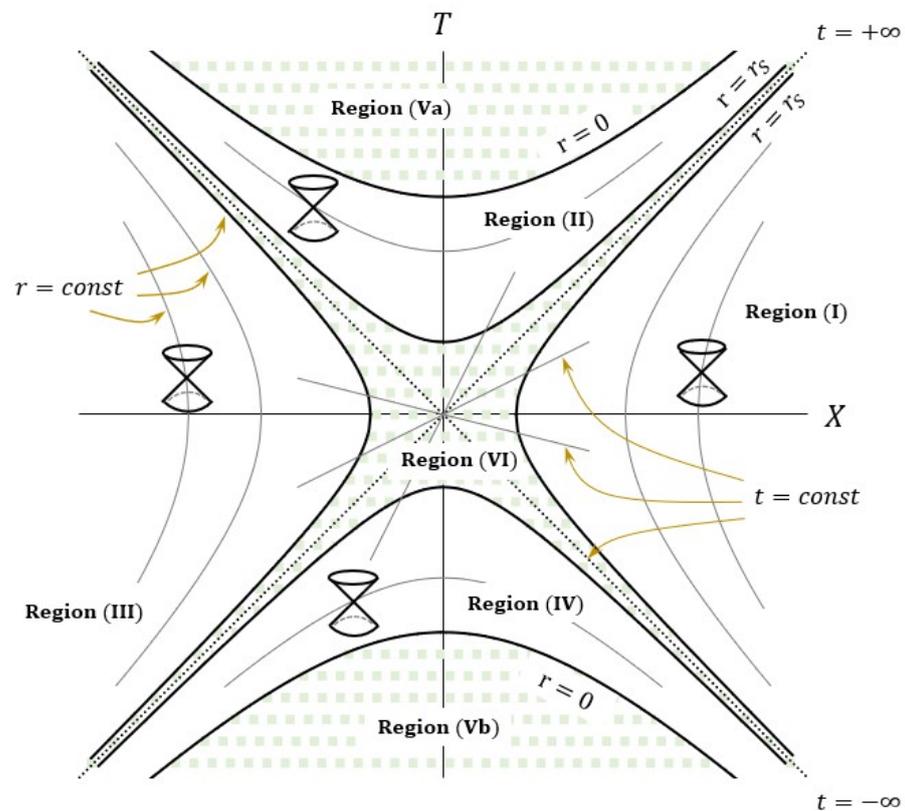
Figure 2. ζ–Kruskal–Szekeres diagrams for the *special* Buchdahl-inspired spacetimes, given by Equation (2) or Equation (9). Each point on the diagram is a 2-sphere. Except for $\tilde{k} = 0$ and $\tilde{k} = -1$, the Kretschmann scalar diverges on the hyperbolae $r = r_s$ and $r = 0$; see Appendix A for exposition.

1. The ζ–KS diagram is conformally Minkowski. The null geodesics are $dX = \pm dT$.
2. Per Equations (20) and (21), a constant–r contour corresponds to a hyperbola, while a constant–t contour corresponds to a straight line running through the origin of the (T, X) plane. The coordinate origin $r = 0$ amounts to $T^2 - X^2 = 1$, since $r^*(r = 0) = 0$.
3. The boundary $r = r_s$ corresponds to *two* distinct hyperbolae, given by

$$T^2 - X^2 = \begin{cases} -e^{-\frac{\pi/\zeta}{\sin(\pi/\zeta)}} & \text{for } r > r_s, \\ +e^{-\frac{\pi/\zeta}{\sin(\pi/\zeta)}} & \text{for } r < r_s. \end{cases} \tag{22}$$

Since each hyperbola has two separate branches on its own, Figure 2 shows four branches representing $r = r_s$ in total. For $\tilde{k} = 0$ (i.e., $\zeta = 1$), the hyperbolic branches (22) degenerate into two straight lines, $T = \pm X$, as is expected for the Schwarzschild metric. In the limit of $\tilde{k} \to 0$, Region (VI), which sandwiches within the four hyperbolic branches, shrinks and disappears.

4. Region (I) refers to $r > r_s$ (the "exterior"); Region (II) refers to $0 < r < r_s$.
5. Regions (III) and (IV) are double copies of Regions (I) and (II) respectively, by flipping the sign of the KS coordinates, viz. $(T, X) \leftrightarrow (-T, -X)$. Regions (Va) and (Vb) are unphysical, viz. $r < 0$.
6. Region (VI) generally contains curvature singularities, with the Kretschmann scalar generally diverging on the hyperbolic branches given in (22). The "gulf" represented by Region (VI) is a new feature of the asymptotically flat Buchdahl-inspired spacetimes. The Kretschmann invariant is reproduced in Appendix A.

Areal Radius

The ζ–KS diagram, depicted in Figure 2, is the maximal analytic extension of the *special* Buchdahl-inspired metric, given in Equation (9). Similar to the usual KS diagram for the Schwarzschild metric, our ζ–KS diagram reveals a double-cover, comprising Regions (III) and (IV).

In [22], one of the present authors showed that, in certain situations, Region (I) and its double-cover Region (III) can be further split. When this splitting occurs, the physical singularities on the hyperbolic branches of $r = r_s$ are shielded from an observer situated at spatial infinity, and the double covers that are connected to spatial infinity can be seamlessly "glued" together to form a two-way traversable wormhole. This procedure was carried out in [22]. However, we shall briefly review the analysis here, for self-consistency and self-completeness.

From Equation (9), the areal radius is given by

$$R(r) = r \left| 1 - \frac{r_s}{r} \right|^{\frac{1}{2}\left(1 + \frac{\tilde{k}-1}{\zeta}\right)} \tag{23}$$

Figure 3 depicts R as function for r for various values of $\tilde{k}$. Furthermore, since

$$\frac{dR}{dr} = \frac{r - \left(\frac{1}{2} - \frac{\tilde{k}-1}{2\zeta}\right)r_s}{r - r_s} \left| 1 - \frac{r_s}{r} \right|^{\frac{1}{2}\left(1 + \frac{\tilde{k}-1}{\zeta}\right)}, \tag{24}$$

the equation $dR/dr = 0$ has a single root, given by

$$r_* = \frac{r_s}{2} \left(1 - \frac{\tilde{k}-1}{\zeta} \right). \tag{25}$$

This root lies in the range of (r_s, ∞) as a local minimum if $\tilde{k} \in (-1, 0)$ and in the range of $(0, r_s)$ as a local maximum if $\tilde{k} \in (-\infty, -1) \cup (0, +\infty)$. We refer the reader to Figure 3 for more details, and below, we briefly analyze both cases.
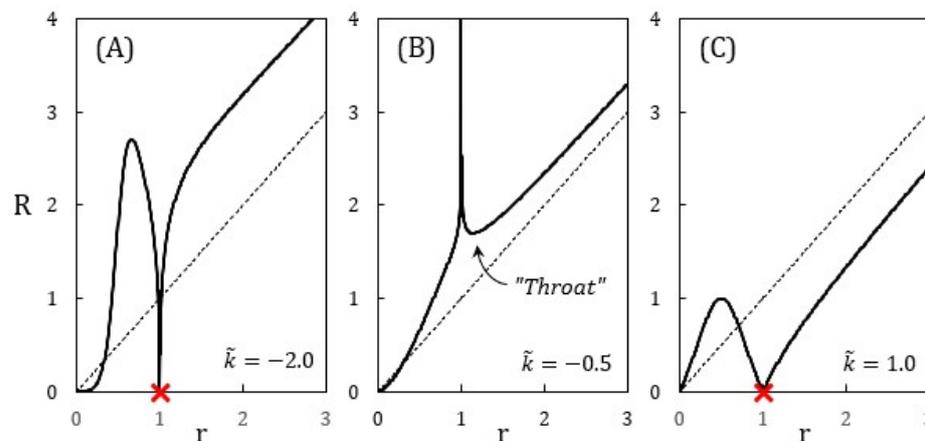

Figure 3. R vs. r for the *special* Buchdahl-inspired metric; using $r_s = 1$. Panel (**B**), representative of $\tilde{k} \in (-1, 0)$, yields a minimum for $R(r)$ and corresponds to a wormhole. Panels (**A**,**C**), representative of $\tilde{k} \in (-\infty, -1) \cup (0, +\infty)$, show a monotonic behavior for $R(r)$ in the "exterior", $r > r_s$.

5. Naked Singularity: Case $\tilde{k} \in (-\infty, -1) \cup (0, +\infty)$

This case corresponds to Figure 3A,C. The "exterior" Region (I) forms one continuous sheet, and its double cover Region (III) forms another continuous sheet.

We plot a timelike trajectory $A \to B$ in Figure 4. In Region (I), an infalling traveller reaches the singularity at point B after a finite amount of proper time. Note that in the view of an observer who stays at rest at spatial infinity in Region (I), it takes a finite amount of time t for the traveller to hit the singularity. This is *in contrast to* the Schwarzschild metric, where an observer from afar will never witness the traveller reaching the horizon at $r = r_s$.

What happens to the traveller after reaching the singularity remains an open question with several possibilities. There are at least three scenarios to consider: (i) the traveller might come to a halt at $r = r_s$ without further motion; (ii) the traveller might enter the "gulf" region, viz. Region (VI); or (iii) the traveller might directly pass into Region (II) and continue heading towards the singularity at $r = 0$. Regardless of the outcome, we do not concern ourselves with this case. Our focus is directed towards the wormhole scenario, which will be presented next.
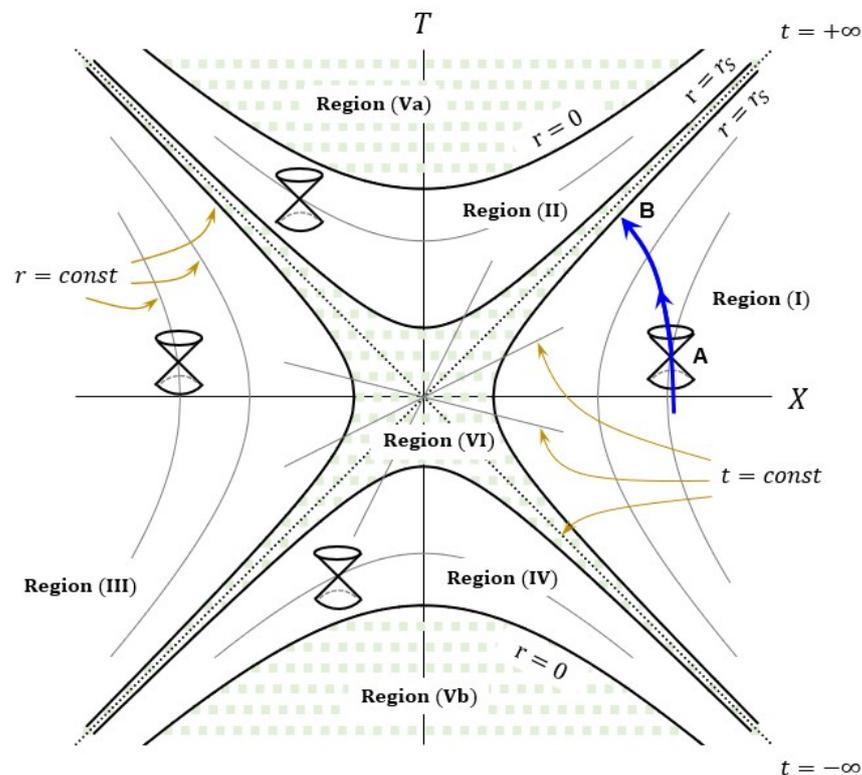

Figure 4. The case of naked singularities, $\tilde{k} \in (-\infty, -1) \cup (0, +\infty)$. On the infalling radial timelike trajectory (blue line), a particle in Region (I) eventually hits the naked singularity at $r = r_s$.

6. Wormhole: Case $\tilde{k} \in (-1, 0)$

Panel (B) in Figure 3 is representative of this case. The areal radius R exhibits a minimum at $r_* = \frac{r_s}{2} \left(1 - \frac{\tilde{k}-1}{\zeta}\right)$ in the "exterior" region, viz. $r_* > r_s$, per Equation (25). In Ref. [22], this fact was employed to construct a Morris–Thorne–Buchdahl (MTB) wormhole with its throat located at r_*. A schematic depiction of the wormhole at a specific time-slice (at a given T), with the azimuth angle φ shown and the polar angle θ suppressed, is shown in Figure 5. We refer the reader to Ref. [22] for details.

The ζ–KS diagram exhibits an additional feature: in Figure 6, the loci where $r = r_*$, representing the local minimum areal radius, are depicted as two thick red hyperbolic branches. These branches partition the "exterior" Region (I) into two sub-regions, denoted as (Ia) and (Ib), while the double-cover Region (III) is also divided into two sub-regions, (IIIa) and (IIIb). The two asymptotically flat sheets in sub-region (Ia) and sub-region (IIIa)

are seamlessly connected or "glued" together along the two thick red hyperbolic branches (as well as along the polar angle θ and the azimuth angle φ of the two-sphere) to form a four-dimensional wormhole.
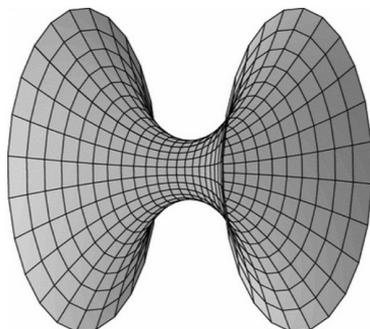
Figure 5. Embedding diagram of a typical traversable wormhole. The wormhole "throat" is depicted horizontally to be compatible with Figure 6 on page 9, with the right mouth corresponding to Region (Ia) and the left mouth Region (IIIa). Note, however, that the embedding diagram is a "snapshot" at a fixed timeslice T (while the azimuth direction is made explicit), whereas the ζ–KS shows the full "evolution" in the T−direction (with both the polar and azimuth angles being suppressed).
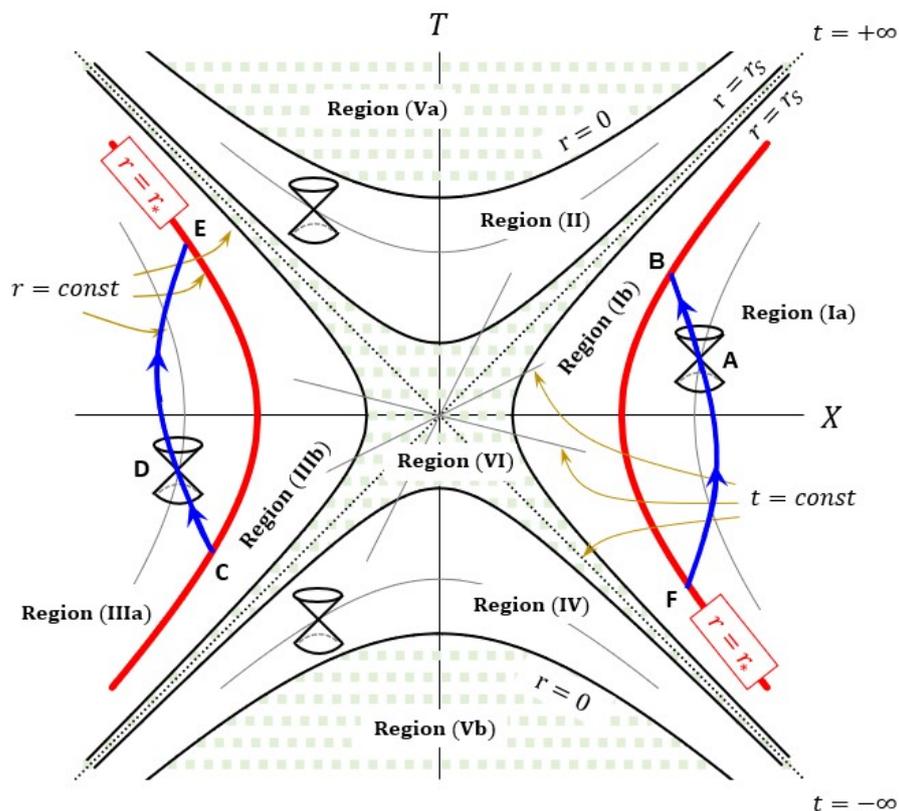
Figure 6. The case of the traversable wormhole, with $\tilde{k} \in (-1, 0)$. The wormhole throat is depicted by the red lines, which further split Region (I) into (Ia) and (Ib), and Region (III) into (IIIa) and (IIIb). On the radial trajectory $A \to B \equiv C \to D \to E \equiv F \to A$, an infalling traveller in sub-region (Ia) first enters the wormhole mouth at point B then traverses into sub-region (IIIa) by emerging at the other mouth at point C (hence, on outgoing motion). As the two red lines are "glued" together to form a wormhole that connects sub-region (Ia) and sub-region (IIIa), the pair of antipodal points B and C represent a single spacetime event. Likewise, the pair of antipodal points E and F correspond to a single spacetime event. The segment $C \to D \to E$ progresses *backward* in time as compared with the segment $F \to A \to B$.

It is essential to note that, according to Equations (20) and (21), each spacetime event (t, r) with r in the range of (r_s, ∞) corresponds to two antipodal points (T, X) and $(-T, -X)$ of the KS coordinates. This duplication (or double degeneracy) is nothing but a double copy of exterior sheets. However, in general, these two points correspond to distinct spacetime events which occur in two separate sheets. *Only along the loci $r = r_*$ do the sheets become "glued" together, forming a wormhole throat with the two thick red hyperbolic branches as the two mouths. Along the throat, the two antipodal points correspond to the same spacetime event.* In other words, in Figure 6, point B and point C are identical, as are points E and F. Note that this identification does *not* apply, for instance, to the pair of antipodal points A and D, as *these points stay off the throat*. That is to say, despite sharing the same value of r and the same value of t, point A and point D represent two independent events that take place in two separate spacetime sheets.

The identification of antipodal points *on the throat* can be illuminated by examining the proper radial coordinate. This coordinate is expressible using Gaussian hypergeometric functions, with $\zeta := \sqrt{1 + 3\tilde{k}^2}$ and $B := (\tilde{k} - 1)/\zeta$, as derived in [22]:
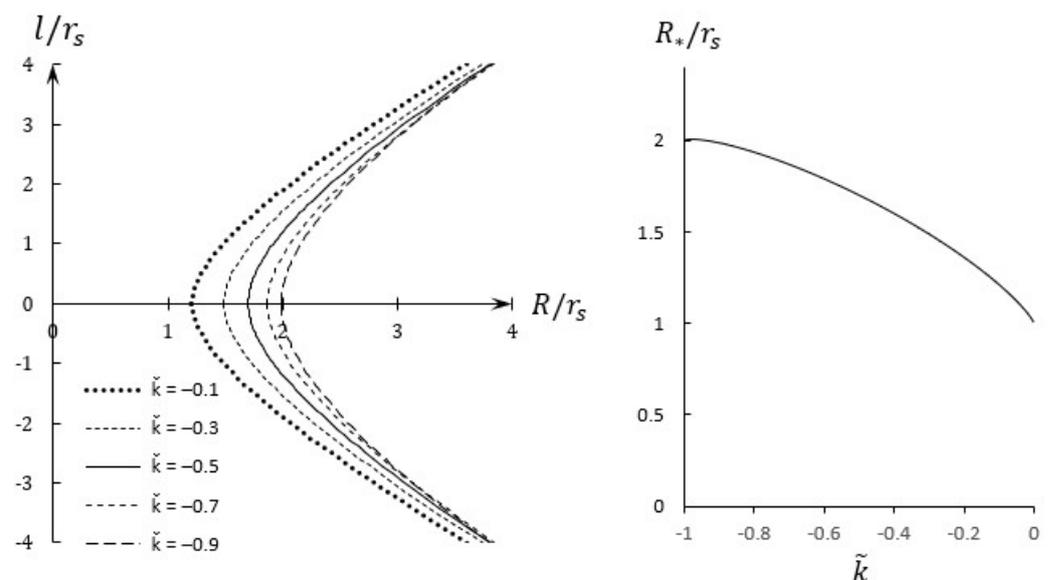
$$l(R) = \pm \int_{R_*}^{R} \frac{dR}{\sqrt{1 - \frac{b(R)}{R}}} \tag{26}$$

$$= \pm \frac{\zeta\, r_s}{1 + \frac{B}{2}} \times \left[y^{1 + \frac{B}{2}} {}_2F_1\left(2, 1 + \frac{B}{2}; 2 + \frac{B}{2}; y\right) - y_*^{1 + \frac{B}{2}} {}_2F_1\left(2, 1 + \frac{B}{2}; 2 + \frac{B}{2}; y_*\right) \right] \tag{27}$$

where the areal radius is given by

$$R(y) = \zeta\, r_s \frac{y^{\frac{1}{2}(B+1)}}{1 - y} \tag{28}$$

Figure 7 illustrates the proper radial coordinate for various values of $\tilde{k}$ within the range $(-1, 0)$. For instance, when $\tilde{k} = -0.5$, it corresponds to $B \approx -1.134$, $y_* \approx 0.0628$, $r_* \approx 1.14\, r_s$, $R_* \approx 1.7\, r_s$.

Figure 7. (**Left**): Proper radial coordinate as a function of areal radius for various value of $\tilde{k} \in (-1, 0)$, per Equations (27) and (28). Each curve is *vertical* at $l = 0$, the location of a wormhole throat. (**Right**): The size of the throat as a function of $\tilde{k} \in (-1, 0)$.

In Figure 7, for a given $\tilde{k} \in (-1, 0)$, the curve of $l(R)$ consists of two semi-infinite segments: The segment with $l > 0$ corresponds to Region (Ia), whereas the segment with

$l < 0$ to Region (IIIa) in the ζ–KS diagram of Figure 6. These two segments are connected at the throat, marked by $l = 0$ and $R = R_*$ (the minimum in the real radius), at which point the curve $l(R)$ is *vertical*. It is only at this specific juncture that the two asymptotic flat sheets, viz. Regions (Ia) and (IIIa), "touch" each other, allowing a transition from one sheet to another and enabling the identification of antipodal points to take effect.

The coordinate l covers the entire range $(-\infty, +\infty)$. A geodesic running across the throat is thus *complete*, without encountering any physical singularities. As the MTB wormhole consists of Regions (Ia) and (IIIa), the physical singularities located at $r = r_s$ are insulated within Regions (Ib) and (IIIb), which are not components of the wormhole.

Now, consider an intrepid traveller tracking an infall starting from point A:

- The traveller enters the right mouth of the wormhole at point B after a finite amount of proper time. From the perspective of an observer at rest in Region (Ia), it also takes a *finite* amount of time for the traveller to reach point B.
- Subsequently, the traveller emerges from the left mouth of the wormhole at point C (note: point B and point C are identical!). They then ascend the potential well (viz. *increasing r*), moving toward point D. It is important to note that, relative to the observer in Region (Ia), the traveller appears to move *backward* in time, as the t coordinate *decreases* from point C to point D.
- If the traveller chooses to fall back into the left mouth, they will re-enter it at point E. They will then re-emerge at the right mouth at point F (which is identical to point E!). Notably, upon re-emergence, they are once again moving *forward* in time.
- At this stage, the traveller can choose to proceed to point A, thereby *completing a closed timelike loop*.

The traveller's ability to complete such a loop relies on the *two reversals of time direction*, occurring each time they enter a wormhole mouth and emerges from the other mouth.

7. Discussions and Summary

In the preceding section, we have constructed a closed timelike curve (CTC) by having a traveller pass through the wormhole throat twice in succession. During each passage, the traveller experiences a reversal in the time direction *with respect to* an observer at rest. This construction is succinctly captured in Figure 6, where the closed path $A \to B \equiv C \to D \to E \equiv F \to A$ forms a CTC.

1. It is worth highlighting that the CTC we have described does not require having one wormhole mouth move at high speed or be located near a supermassive object to accumulate time dilation, as popularized in [2,6,19]. To the best of our knowledge, the CTC presented herewith has not been documented in the existing literature.

2. Our association of a pair of antipodal points (such as B and C) with a single spacetime event was inspired by a similar construction proposed by Popławski. In [23], he revisited the Einstein–Rosen (ER) bridge and identified two antipodal points *on the horizon* with a single spacetime event. The ER bridge was interpreted as a "Schwarzschild wormhole" connecting the two exterior sheets joined *at the horizon*. However, the ER bridge encounters various issues related to traversability, stability, and a problematic thin-shell mass distribution at the horizon. (It is also worth noting that Popławski did not suggest the possibility of CTCs in his work.)

3. The Morris–Thorne–Buchdahl wormhole, developed in [22] and briefly summarized in this paper, appears to avoid the issues faced in Popławski's work. Setting aside the *physical* questions regarding causality violations and time-travel-related paradoxes, our construction of a CTC appears to be *mathematically* consistent.

4. Central to our approach is the identification of any given pair of antipodal points on the loci of minimum areal radius, denoted as $r = r_*$, with a single spacetime event. This identification becomes evident through Equations (20) and (21), as well as in the KS diagrams employed for the Schwarzschild metric (used in Popławski's work) and our *special* Buchdahl-inspired metric in Figure 6.

5. Embedding diagrams, such as the one in Figure 5, depict a "snapshot" of the wormhole at a fixed timeslice, without illustrating the evolution of timelike trajectories. As such, the use of embedding diagrams may obscure the identification of spacetime events on the throat, a procedure we carried out in this paper. In this regard, the decisive advantage of KS diagrams is their ability to reveal the full causal structure of spacetime, making this identification transparent.

6. Let us draw a comparison between our CTC and the Deutsch-Politzer (DP) time machine.

   - In [27,28], a DP space is created from a two-dimensional Minkowski spacetime by making two finite-size "space-like" cuts and gluing the edges of the cuts, effectively forming a "handle" which connects two space-like regions and creates a time machine. The essence of a DP time machine is that *the spacetime topology is altered* [Note that the DP space has singularities; to exorcise them, in [29,30] Krasnikov performed a conformal transformation to send the singular points away to infinity].

   - Our CTC construction shares both analogies and differences with the DP time machine. The ζ–KS diagram of the Buchdahl-inspired vacuum (Figure 6) is a two-dimensional Minkowski spacetime (modulo a Weyl transformation). For $\tilde{k} \in (-1, 0)$, the hyperbolic branches of $r = r_*$ are glued to form a portal between the two time-reversed sheets, viz. Regions (Ia) and (IIIa). *In this regard, akin to the DP space, our construction is a concrete realization of a time machine induced by an alteration in the topology of spacetime.*

   - Unlike the deliberate surgery employed in the DP space, the alteration of the topology in the Buchdahl-inspired vacuum occurs naturally, driven by the fourth-derivative dynamics of pure $\mathcal{R}^2$ gravity. (Also, similar to Krasnikov's work [29,30], Regions (Ia) and (IIIa) in our ζ–KS diagram are devoid of (physical) singularities.) A comprehensive discussion of their commonalities and differences exceeds the scope of this paper.

7. Our CTC construction is not confined solely to the MTB wormholes of pure $\mathcal{R}^2$ gravity. It is also applicable to two-way traversable wormholes in Brans–Dicke (BD) gravity, which share a similar Kruskal–Szekeres diagram, as demonstrated in Ref. [24] by one of the authors.

   - More generally, the Brans wormhole, first established by Agnese and La Camera for BD gravity in [31,32], encompasses the MTB wormhole in $\mathcal{R}^2$ gravity [24]. It is known that a static vacuum solution of any $f(R)$ gravity cannot host a twice asymptotically flat wormhole [33]. However, a cut-and-paste procedure can be employed to generate such a wormhole, a technique that underlies the creation of the Brans wormhole [31,32,34,35].

   - The MTB wormhole satisfies the four "traversability-in-principle" criteria laid out by Morris and Thorne [1]. To be considered "usable", the tidal forces should remain finite. We have computed the tidal forces in Appendix B. Our findings indicate that despite jumps in higher derivatives across the throat in the metric components, the tidal forces remain finite throughout the two asymptotically flat spacetime sheets.

In conclusion, the presence of CTCs is an extremely subtle issue which needs to be handled with great caution, due to the association with time travel paradoxes, such as the classical consistency paradoxes and causal loops [19]. Much has been written on the resolution to the paradoxes associated with CTCs, such as the Principle of Self-Consistency [36–38] and the Chronology protection conjecture [39] (we refer the reader to [19] for more details). The issue of CTCs is an extremely fascinating research topic and is essentially useful as "gedanken-experiments" that force us to confront the foundations of general relativity, and its modifications, and extract clarifying views.

Appendix A. Kretschmann Scalar

The Kretschmann invariant has been computed in [24,40]

$$K := \mathcal{R}_{\mu\nu\rho\sigma}\mathcal{R}^{\mu\nu\rho\sigma} \tag{A1}$$

$$= \left|1 - \frac{r_{\rm s}}{r}\right|^{-\frac{2}{\zeta}(\tilde{k}-1+2\zeta)} \frac{r_{\rm s}^2}{r^6}\left(6\mathfrak{A} - 2\mathfrak{B}\frac{r_{\rm s}}{r} + \frac{\mathfrak{C}}{4}\frac{r_{\rm s}^2}{r^2}\right) \tag{A2}$$

in which $A := \frac{\tilde{k}+1}{\zeta}$, $B := \frac{\tilde{k}-1}{\zeta}$, $\zeta := \sqrt{1+3\tilde{k}^2}$, whereas

$$\mathfrak{A} = A^2 + B^2 \tag{A3}$$

$$\mathfrak{B} = A^2(A - 2B + 3) - B(B-1)(B-2) \tag{A4}$$

$$\mathfrak{C} = (A+1)A^2(A - 2B + 3) + (3A^2 + B^2 - 2B + 3)(B-1)^2 \tag{A5}$$

- At $\tilde{k} = 0$: $\zeta = 1$, $\mathfrak{A} = 2$, $\mathfrak{B} = 12$, $\mathfrak{C} = 48$, giving $K = 12\frac{r_{\rm s}^2}{r^6}$ in agreement with the standard result fort the Schwarzschild metric.
- At $\tilde{k} = -1$: $\zeta = 2$, $\mathfrak{A} = 1$, $\mathfrak{B} = 6$, $\mathfrak{C} = 24$, giving $K = 6\frac{r_{\rm s}^2}{r^6}$.
- For $\tilde{k} \neq 0$ and $\tilde{k} \neq -1$, as $\tilde{k} - 1 + 2\zeta > 0$, K generally diverges at $r = r_{\rm s}$ and $r = 0$.

Appendix B. Tidal Forces in MTB and Brans Wormholes

In addition to the four "traversability-in-principle" criteria [1], it is desirable to require that the metric components be at least twice-differentiable in terms of the radial coordinate [41]. This "usability" requirement *may* be justified since the tidal forces, which are the physical quantities of concern, involve the first and second derivatives of the redshift and shape functions (as we shall see momentarily). Let us compute the tidal forces for the Morris–Thorne–Buchdahl (MTB) wormholes and the Brans wormholes.

We shall adopt Morris–Thorne (MT)'s exposition [1]. For the MT ansatz

$$ds^2 = -e^{2\Phi(R)}dt^2 + \frac{dR^2}{1 - \frac{b(R)}{R}} + R^2 d\Omega^2 \tag{A6}$$

the radial and lateral tidal forces are proportional to (with primes denoting derivatives with respect to R):

$$|\mathcal{R}_{\hat{1}'\hat{0}'\hat{1}'\hat{0}'}| = \left| \left(1 - \frac{b}{R} \right) \left(-\Phi'' + \frac{b'R - b}{2R(R - b)} \Phi' - \Phi'^2 \right) \right| \tag{A7}$$

$$= \left| \left(1 - \frac{b}{R} \right) \left(-\Phi'' - \Phi'^2 \right) - \left(1 - \frac{b}{R} \right)' \frac{\Phi'}{2} \right| \tag{A8}$$

$$|\mathcal{R}_{\hat{2}'\hat{0}'\hat{2}'\hat{0}'}| = \left| \frac{\gamma^2}{2R^2} \left[\frac{v^2}{c^2} \left(b' - \frac{b}{R} \right) + 2(R - b)\phi' \right] \right| \tag{A9}$$

$$= \left| \frac{\gamma^2}{2R} \left[-\frac{v^2}{c^2} \left(1 - \frac{b}{R} \right)' + 2 \left(1 - \frac{b}{R} \right) \phi' \right] \right| \tag{A10}$$

These expressions are Equations (49) and (50) in the MT paper [1]. It thus appears desirable to impose twice-differentiability on Φ and first-differentiability on b as functions of R.

Let us apply these formulae for the asymptotically flat Buchdahl-inspired solution [22] and the Campanelli–Lousto solution [24,31]. Both of these solutions can be cast in the MT ansatz, Equation (A6), in which the redshift and shape functions are [22]

$$e^{2\Phi(R)} = y^A \tag{A11}$$

$$1 - \frac{b(R)}{R} = \frac{(1 - B)^2}{4y} \left(y - \frac{B + 1}{B - 1} \right)^2 \tag{A12}$$

in which the auxiliary variable $y := \left(1 - \frac{r_s}{r} \right)^\zeta \in (0, 1)$ and the areal radius R is expressed as

$$R(y) = \zeta r_s \frac{y^{\frac{1}{2}(B+1)}}{1 - y}. \tag{A13}$$

For the Campanelli–Lousto solution, A and B are two independent parameters, while $\zeta := 1$ [24,31]. For the asymptotically flat Buchdahl-inspired solution, A and B are related by the following definitions [22]

$$A := \frac{\tilde{k} + 1}{\zeta}; \ \ B := \frac{\tilde{k} - 1}{\zeta}; \ \ \zeta := \sqrt{1 + 3\tilde{k}^2} \tag{A14}$$

As demonstrated in Ref. [22], for $\tilde{k} \in (-1, 0)$, the areal radius has a minimum at

$$y_* := \frac{B + 1}{B - 1} \in (0, 1) \tag{A15}$$

This is the location of the throat, and the variable y for *both* of the two spacetime sheets are in the range $[y_*, 1)$.

Direct calculations yield:

$$\left(1 - \frac{b}{R} \right)' = \frac{(1 - B)y^{-\frac{1}{2}(B+3)}(1 - y)^2}{2\zeta r_s} \left(y + \frac{B + 1}{B - 1} \right) \tag{A16}$$

$$\left(1 - \frac{b}{R} \right) \Phi' = \frac{A(1 - B)y^{-\frac{1}{2}(B+3)}(1 - y)^2}{4\zeta r_s} \left(y - \frac{B + 1}{B - 1} \right) \tag{A17}$$

$$\left(1 - \frac{b}{R} \right) \left(-\Phi'' - \Phi'^2 \right) - \left(1 - \frac{b}{R} \right)' \frac{\Phi'}{2} = \frac{A(2 + A - B)y^{-B-2}(1 - y)^3}{4\zeta^2 r_s^2} \times$$
$$\left(y - \frac{B - A + 2}{B - A - 2} \right) \tag{A18}$$

Since all these expressions do not contain any singularity for $y \in [y_*, 1)$, *the tidal forces in Equations* (A8) *and* (A10) *are finite everywhere in this range.* It is important to note that the

tidal forces may have opposite signs in the two sheets across the throat, but *they remain finite* on the two asymptotically flat sheets that form the MTB wormhole.

Furthermore, it should be noted that all the calculations between Equations (A15) and (A18) are extendible to the Campanelli–Lousto solution provided that $B < -1$, in which case a Brans wormhole has been established to exist [24,31]. Our conclusion regarding the finite tidal forces is therefore applicable to Brans wormholes as well.

References

1. Morris, M.S.; Thorne, K.S. Wormholes in spacetime and their for interstellar travel: A tool for teaching general relativity. *Am. J. Phys.* **1988**, *56*, 395. [CrossRef]
2. Visser, M. *Lorentzian Wormholes: From Einstein to Hawking*; Springer: New York, NY, USA, 1996; ISBN 9781563966538.
3. Alcubierre, M.; Lobo, F.S.N. Wormholes, Warp Drives and Energy Conditions. *Fundam. Theor. Phys.* **2017**, *189*, 257–279.
4. Lobo, F.S.N.; Oliveira, M.A. Wormhole geometries in $f(R)$ modified theories of gravity. *Phys. Rev. D* **2009**, *80*, 104012. [CrossRef]
5. Harko, T.; Lobo, F.S.N.; Mak, M.K.; Sushkov, S.V. Modified-gravity wormholes without exotic matter. *Phys. Rev. D* **2013**, *87*, 067504. [CrossRef]
6. Morris, M.S.; Thorne, K.S.; Yurtsever, U. Wormholes, Time Machines, and the Weak Energy Condition. *Phys. Rev. Lett.* **1988**, *61*, 1446. [CrossRef] [PubMed]
7. Novikov, I.D. An analysis of the operation of a time machine. *Sov. Phys. JETP* **1989**, *68*, 3.
8. Frolov, V.P.; Novikov, I.D. Physical effects in wormholes and time machines. *Phys. Rev. D* **1990**, *42*, 1057. [CrossRef] [PubMed]
9. Friedman, J.L.; Morris, M.S.; Novikov, I.D.; Echeverria, F.; Klinkhammer, G.; Thorne, K. S.; Yurtsever, U. Cauchy problem in spacetimes with closed timelike curves. *Phys. Rev. D* **1990**, *42*, 1915. [CrossRef]
10. Gödel, K. An Example of a New Type of Cosmological Solution of Einstein's Field Equations of Gravitation. *Rev. Mod. Phys.* **1949**, *21*, 447. [CrossRef]
11. Pfarr, J. Time travel in Gödel's space. *Gen. Rel. Grav.* **1981**, *13*, 1073. [CrossRef]
12. Tipler, F.J. Causality violation in asymptotically flat space-times. *Phys. Rev. Lett.* **1976**, *37*, 879. [CrossRef]
13. de Felice, F.; Calvani, M. Time machine and geodesic motion in Kerr metric. *Gen. Rel. Grav.* **1978**, *9*, 155.
14. Gott, J.R. Closed Timelike Curves Produced by Pairs of Moving Cosmic Strings: Exact Solutions. *Phys. Rev. Lett.* **1991**, *66*, 1126. [CrossRef] [PubMed]
15. Ori, A. Must time machine construction violate the weak energy condition? *Phys. Rev. Lett.* **1993**, *71*, 2517. [CrossRef] [PubMed]
16. Ori, A. A class of time-machine solutions with a compact vacuum core. *Phys. Rev. Lett.* **2005**, *95*, 021101. [CrossRef]
17. Alcubierre, M. The warp drive: Hyperfast travel within general relativity. *Class. Quant. Grav.* **1994**, *11*, L73. [CrossRef]
18. Everett, A.E. Warp drive and causality. *Phys. Rev. D* **1996**, *53*, 7365. [CrossRef] [PubMed]
19. Lobo, F.S.N. Closed timelike curves and causality violation. *arXiv* **2010**, arXiv:1008.1127.
20. Nguyen, H.K. Beyond Schwarzschild-de Sitter spacetimes: II. An exact non-Schwarzschild metric in pure R^2 gravity and new anomalous properties of R^2 spacetimes. *Phys. Rev. D* **2023**, *107*, 104008. [CrossRef]
21. Buchdahl, H.A. On the Gravitational Field Equations Arising from the Square of the Gaussian Curvature. *Nuovo Cimento* **1962**, *23*, 141. [CrossRef]
22. Nguyen, H.K.; Azreg-Aïnou, M. Traversable Morris-Thorne-Buchdahl wormholes in quadratic gravity. *Eur. Phys. J. C* **2023**, *83*, 626. [CrossRef]
23. Popławski, N.J. Radial motion motion into an Einstein–Rosen bridge. *Phys. Lett. B* **2010**, *687*, 110. [CrossRef]
24. Nguyen, H.K.; Azreg-Aïnou, M. Revisiting Weak Energy Condition and wormholes in Brans-Dicke gravity. *arXiv* **2023**, arXiv:2305.15450.
25. Nguyen, H.K. Beyond Schwarzschild-de Sitter spacetimes: A new exhaustive class of metrics inspired by Buchdahl for pure R^2 gravity in a compact form. *Phys. Rev. D* **2022**, *106*, 104004. [CrossRef]
26. Nguyen, H.K. Buchdahl-inspired spacetimes and wormholes: Unearthing Hans Buchdahl's other 'hidden' treasure trove. *Int. J. Mod. Phys. D* **2023**, 2342007. [CrossRef]
27. Deutsch, D. Quantum mechanics near closed timelike lines. *Phys. Rev. D* **1991**, *44*, 3197. [CrossRef]
28. Politzer, H.D. Simple quantum systems in spacetimes with closed timelike curves. *Phys. Rev. D* **1992**, *46*, 4470. [CrossRef]
29. Krasnikov, S.V. A singularity-free WEC-respecting time machine. *Class. Quant. Grav.* **1998**, *15*, 997. [CrossRef]
30. Krasnikov, S.V. Topology Change without any Pathology. *Gen. Rel. Gravit.* **1995**, *27*, 529. [CrossRef]
31. Agnese, A.G.; La Camera, M. Wormholes in the Brans-Dicke theory of gravitation. *Phys. Rev. D* **1995**, *51*, 2011. [CrossRef]
32. Agnese, A.G.; La Camera, M. Schwarzschild metrics, quasi-universes and wormholes. In *Frontiers of Fundamental Physics 4*; Sidharth, B.G., Altaisky, M.V., Eds.; Kluwer Academic/Plenum Publishers: New York, NY, USA, 2001; p. 197.
33. Bronnikov, K.A.; Skvortsova, M.V.; Starobinsky, A.A. Notes on wormhole existence in scalar-tensor and $F(R)$ gravity. *Grav. Cosmol.* **2010**, *16*, 216. [CrossRef]
34. Nandi, K.K.; Islam, A. Brans wormhole. *Phys. Rev. D* **1997**, *55*, 2497. [CrossRef]
35. Vanzo, L.; Zerbini, S.; Faraoni, V. Campanelli-Lousto and veiled spacetimes. *Phys. Rev. D* **2012**, *86*, 084031. [CrossRef]
36. Earman, J. *Bangs, Crunches, Whimpers, and Shrieks: Singularities and Acausalities in Relativistic Spacetimes*; Oxford University Press: Oxford, UK, 1995.

37. Echeverria, F.G.; Klinkhammer, G.; Thorne, K.S. Billiard Balls in Wormhole Spacetimes with Closed Timelike Curves: Classical Theory. *Phys. Rev. D* **1991**, *44*, 1077. [CrossRef]
38. Novikov, I.D. Time machine and self-consistent evolution in problems with self-interaction. *Phys. Rev. D* **1992**, *45*, 1989. [CrossRef] [PubMed]
39. Hawking, S.W. Chronology protection conjecture. *Phys. Rev. D* **1992**, *46*, 603. [CrossRef]
40. Bronnikov, K.A; Constantinidis, C.P.; Evangelista, R.L.; Fabris, J.C. Cold black holes in scalar-tensor theories. *arXiv* **1997**, arXiv:gr-qc/9710092.
41. Visser, M.; Hochberg, D. Generic wormhole throats. *Ann. Isr. Phys.* **1997**, *13*, 249.